Synthesis of a gallium-functionalized polyoxovanadate-alkoxide cluster: Toward a general route for heterometal installation

*Rachel L. Meyer,[a] William W. Brennessel,[a] and Ellen M. Matson[a]**

[a] Department of Chemistry, University of Rochester, Rochester, New York 14627, United States

ABSTRACT.

Incorporating transition metal ions into Lindqvist polyoxovanadate-alkoxide (POV-alkoxide) clusters has been shown to be an effective method for tuning the electronic properties of these molecular assemblies. Herein, we report the synthesis of a gallium-functionalized POV-alkoxide cluster, extending the family of heterometal-functionalized clusters to a metalloid ion. Complex $[V_5O_6(OCH_3)_{12}GaCl]$ was characterized by infrared and electronic absorption spectroscopies and cyclic voltammetry, revealing the retention of the extensive delocalization upon installation of the $3d^{10}$ ion. The new reaction conditions developed for $[V_5O_6(OCH_3)_{12}GaCl]$ were shown to successfully generate the iron analogue, $[V_5O_6(OCH_3)_{12}FeCl]$, from a ferric salt precursor. However, attempts at installing other group 13 ions, e.g. In^{III}, instead produced the cyclic hexavanadate cluster, $[Bu_4N][V_6O_6(OCH_3)_{12}Cl]$.

INTRODUCTION.

Polyoxometalates (POMs) are molecular metal oxide clusters that contain three or more transition metals ions, typically tungsten, molybdenum, and vanadium, bridged by shared oxygen atoms.[1-3] These three-dimensional molecular assemblies exhibit a range of structural and electronic properties, due to their wide diversity in size, morphology, and composition. POMs can be divided into two broad categories based on their chemical makeup: 1) homometallic, where the metal oxide assembly contains only one metal-type, and 2) heterometallic, where heteroatom(s) (e.g. p-block elements other than oxygen and transition and f-block metals) are incorporated into the cluster.[2-3] The synthesis of heterometallic POMs are of particular interest, as the heteroion can confer unique structural, electronic, and chemical properties to the metal oxide assemblies, allowing for the systematic design of multifunctional materials. Indeed, researchers have unearthed a variety of applications for heteroatomic POMs, including catalysis,[4-6] photocatalysis,[7-8] materials science,[9] medicinal chemistry,[10-11] molecular magnetism,[12-13] and energy storage.[14-16]

In comparison to heterometallic polyoxotungstates and polyoxomolybdates, heterometal-functionalization of polyoxovanadate (POV) clusters remains underdeveloped (Figure 1).[17] This limited library of heterometallic POVs is due to the structural flexibility of vanadium. Vanadate subunits are capable of adopting a mixture of tetrahedral, square pyramidal, and octahedral coordination geometries within a single cluster, preventing the formation of stable lacunary frameworks that afford facile coordination of a heterometal to the cluster.[17] Consequently, the few examples of lacunary POV clusters that do exist invoke a placeholder strategy, in which cationic subunits stabilize the vacant site.[18-21] As such, the majority of heterometallic vanadium-oxide clusters have been accessed *via* highly variable, self-assembly reactions.[22-31]

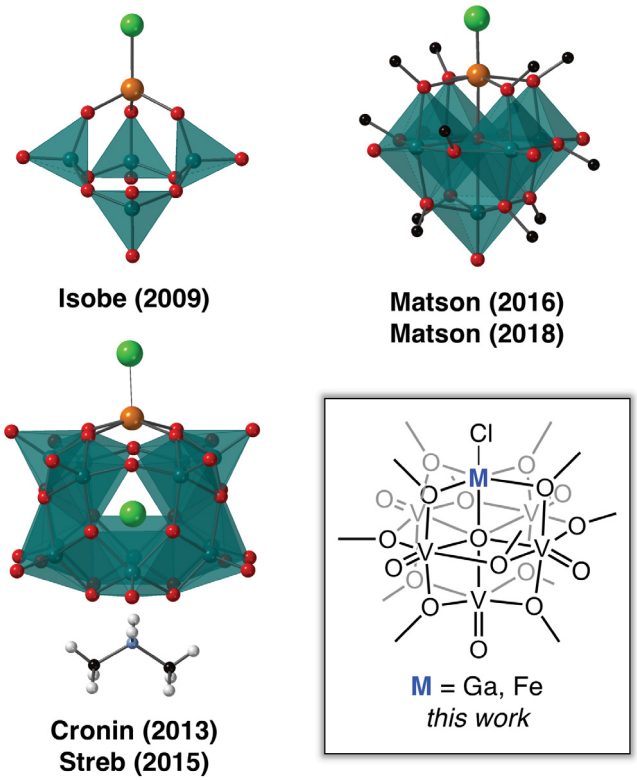

Figure 1. Select examples of heterometallic polyoxovanadate clusters.

An interesting sub-class of POVs are the hexanuclear, polyoxovanadate-alkoxide (POV-alkoxide) clusters $[V_6O_{19-n}(OR)_n]^{m-}$ (R = CH_3, C_2H_5).[32-34] These hexavanadate, Lindqvist assemblies feature monodentate, bridging alkoxide ligands that result in enhanced stability and solubility of the multimetallic assembly. Alkoxo-polyoxovanadium clusters have distinct electronic and magnetic properties, resulting from the mixed-valent nature of vanadyl ions that yield extensive electronic delocalization across the cluster core. Recent studies have demonstrated ligand substitution to be an effective way to modify the solubility and stability of the POV-alkoxide systems.[35-36] However, these modifications leave the electronic structure of the hexavanadate assemblies largely unchanged, prompting interest in developing alternative methods for reliably tuning the physicochemical properties of these systems. Toward this goal, our research laboratory

has been investigating the substitution of a vanadyl cation for an alternative transition metal moiety.

In 2016, our laboratory reported the synthesis of the first heterometal-functionalized POV-alkoxide cluster, namely $[V_5O_6(OCH_3)_{12}FeX]$ (X = Cl, OSO_2CF_3).[30] Subsequently, we demonstrated the retention of the delocalized electronic structure upon substitution of a diverse array of transition metal ions (e. g. M = Ti^{IV}, Zr^{IV}, Hf^{IV}, Fe^{III}).[31] This work established that heteroion substitution serves to modulate the redox potential of the reversible V^{IV}/V^{V} couples within the POV-alkoxide assembly. Heterometal functionalized POV-alkoxide (MPOV-alkoxide) clusters are accessed *via* serendipitous, solvothermal routes. As such, to generate a comprehensive library of heteroatom-functionalized POV-alkoxides, our research group has been investigating the relationship between atomic properties of transition metal ions and main-group elements and their successful incorporation into the Lindqvist core.

Interested in extending our family of MPOV-alkoxide clusters to metalloid-functionalized derivatives, we have been investigating the formation of group 13-substituted polyoxovanadate clusters. Specifically, development of synthetic routes to access a gallium-functionalized POV-alkoxide cluster was of interest, as this metalloid ion has been cited as a redox-innocent substitute for ferric centers in bioinorganic investigations.[37-40] Ga^{III} and Fe^{III} share similar atomic properties, most notably their atomic radii (Ga^{III} = 0.620 Å vs. Fe^{III} = 0.645 Å),[41] suggesting that in analogy to the FePOV-alkoxide cluster previously reported by our laboratory, substitution of a vanadyl ion for a Ga^{III} center would yield a kinetically stable heterometallic cluster. Herein, we report the synthesis and characterization of a gallium-functionalized POV-alkoxide (GaPOV-alkoxide) cluster. This heterometallic structure marks the first example of a gallium-containing POV assembly. This work summarizes the impact the $3d^{10}$ ion has on the physiochemical properties of

the cluster, specifically in comparison to its transition metal-functionalized congeners. Additionally, we report the extension of this synthetic methodology to Fe^{III} and other group 13 ions, affording an opportunity to evaluate the generalizability of the developed reaction conditions.

RESULTS AND DISCUSSION.

Synthesis and Characterization of a Gallium-functionalized POV-alkoxide cluster. In designing a synthetic strategy for the generation of a GaPOV-alkoxide cluster, we considered that mixed-valent, Lindqvist POV-alkoxide clusters typically form under reducing conditions. For example, in the case of the d^0, group 4 ions (e.g. Ti, Zr, Hf), assembly of the heterometal-functionalized POV-alkoxide cluster occurs through the addition of $[Bu_4N][BH_4]$ to the reaction mixture.[31] Like the group 4 ions, the Ga^{III} precursor is a closed shell ion ($3d^{10}$) with limited reducing character. As such, initial attempts at accessing a GaPOV-alkoxide cluster drew inspiration from the synthetic protocols established for the group 4 ions. A 1:5:1 ratio of $GaCl_3$, $VO(OCH_3)_3$, and $[Bu_4N][BH_4]$ in methanol was heated to 100 °C for 24 hr in an autoclave. Analysis of the crude reaction mixture by electrospray ionization mass spectrometry (ESI-MS) and ^1H NMR spectroscopy revealed predominant formation of the homometallic, hexavanadate cluster, $[V_6O_7(OCH_3)_{12}]^-$ (**1-V_6O_7**; *m/z* = 790 amu), with only a small amount of the desired GaPOV-alkoxide, $[V_5O_6(OCH_3)_{12}GaCl]$ (**2-V_5GaCl**; *m/z* = 827/829 amu) (Figure S1).

Encouraged by the formation of some of the desired product, reaction conditions were varied in an attempt to favor production of **2-V_5GaCl**. In our synthesis of iron-functionalized hexavanadate clusters,[30] we noted that lower temperatures afforded isolation of the FePOV-alkoxide species, preventing the generation of **1-V_6O_7**. Lowering the temperature of the gallium reaction to 65 °C increased the amount of **2-V_5GaCl** formed, as observed by ESI-MS (Figure S2).

Additionally, formation of a series of homometallic vanadium byproducts were noted. While lower temperatures seemed to favor production of the desired GaPOV-alkoxide cluster, analysis of the crude reaction mixture by ^{1}H NMR spectroscopy (Figure S2) revealed large amounts of unreacted starting material, $VO(OCH_3)_3$. To drive the reaction to completion, an identical reaction was conducted with two equivalents of $GaCl_3$, increasing the conversion of the mononuclear vanadium precursor. Unfortunately, substantial formation of hexavanadate clusters was still observed (Figure S3).

Challenges in separating the hexavanadate impurities from the GaPOV-alkoxide cluster arose, as a result of the similar solubilities of these molecules. Previously, we reported that attempts to generate FePOV-alkoxide clusters resulted in a mixture of products when self-assembly reactions were conducted in methanol.[30] Instead, the optimal conditions for the assembly of the FePOV-alkoxide cluster were determined to be 85 ^{o}C in toluene. In this reaction, ferrous chloride serves as an "internal" reductant, facilitating direct electron transfer between the iron and vanadium centers. In the case of gallium, the requirement of an external reductant for generation of **2-V_5GaCl** precluded the use of this non-coordinating solvent, as addition of $[Bu_4N][BH_4]$ to a mixture of $GaCl_3$ and $VO(OCH_3)_3$ in toluene results in the precipitation of an unidentified light-purple solid. In order to circumvent the formation of this precipitant, polar aprotic solvents, such as acetonitrile (Figure S4) and tetrahydrofuran (Figure S5), were screened. As observed in the methanol reactions, conducting the identical reaction in acetonitrile resulted in a mixture of inseparable hexavanadate and GaPOV-alkoxide clusters. Fortuitously, when tetrahydrofuran was used as a solvent, selective formation of the **2-V_5GaCl** was achieved.

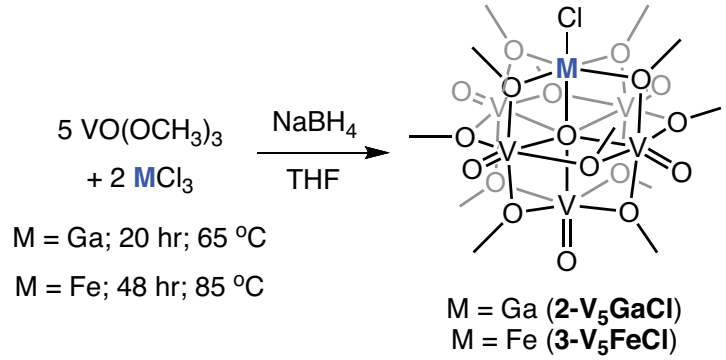

Scheme 1. Synthesis of gallium- and iron-functionalized POV-alkoxide clusters.

While the only vanadium-containing cluster formed under these reaction conditions was the desired GaPOV-alkoxide species, as observed by ^{1}H NMR and ESI-MS, the [Bu_4N][Cl] byproduct was difficult to remove from the product mixture. When $NaBH_4$ was used in the place of [Bu_4N][BH_4], NaCl was formed and was easily separated from **2-V_5GaCl** (Scheme 1). Isolation of the metalloid-functionalized POV-alkoxide cluster was achieved by extracting the product with dichloromethane and filtering the sample over Celite. The purity of complex **2-V_5GaCl** was confirmed by elemental analysis, ^{1}H NMR, and ESI-MS (Figure S6-S7).

Unlike the group 4 derivatives, **2-V_5GaCl** is isolated as a neutral species, with no counter ion associated with the heterometallic cluster. We attribute the differences in overall charge state of these heterometallic clusters to discrepancies in their syntheses. In the case of the group 4 ions, cluster assembly was conducted in methanol at solvothermal temperatures, reaction conditions that are capable of facilitating the reduction of V^{V} ions without an external reductant.[31] In contrast, the preparation of **2-V_5GaCl** occurs in tetrahydrofuran, with $NaBH_4$ as the sole reductant in the reaction mixture.

Considering the neutral charge of complex **2-V_5GaCl** and the static oxidation state of the gallium center (Ga^{III}), charge-balancing can be used to assign oxidation state distributions for the

remaining vanadium ions (e^- distribution: $V^{IV}_3V^V_2Ga^{III}$). The mixed-valent nature of the vanadium ions within complex **2-V_5GaCl** results in extensive delocalization of electron density across the heterometallic core, correlating to a Robin and Day Class II mixed-valent system.[31-34, 42-43] To gain precise spectroscopic insight into the electronic structure of **2-V_5GaCl**, infrared (IR) and electronic absorption spectroscopies were employed (Figure 2, Table 1). The IR spectrum of **2-V_5GaCl** has two intense absorption bands at 1003 and 969 cm^{-1}, corresponding to $\nu(O_b\text{-}OCH_3)$ (O_b = μ^2-oxygen atom of bridging methoxide ligand) and $\nu(V{=}O_t)$ (O_t = terminal oxo), respectively (Figure 2a). These values are in good agreement with those reported for $[V_5O_6(OCH_3)_{12}FeX]$ (X = $OClO_3^-$, $OSO_2CF_3^-$, and OCN^-), clusters which have an analogous charge distribution of metal ions ($V^{IV}_3V^V_2Fe^{III}$). Evidence for the delocalized electronic structure is also obtained from the electronic absorption spectrum of **2-V_5GaCl**, which bears two intervalence charge transfer (IVCT) bands, located at 378 nm (3.4 x 10^3 $M^{-1}cm^{-1}$) and at ~990 nm (3.5 x 10^2 $M^{-1}cm^{-1}$) (Figure 2b). These absorptions are indicative of a mixed-valent POV-alkoxide core, where the higher energy band can be assigned to an electron transfer from $d_{xy}(V^{IV}) \rightarrow d_{x^2-y^2}(V^V)$, and the lower energy absorption is associated with a transition between $d_{xy}(V^{IV}) \rightarrow d_{xy}(V^V)$ orbitals.[33, 42]

To rigorously define the molecular structure of **2-V_5GaCl**, a crystal grown from a concentrated solution of dibutyl ether at -30 °C was analyzed by X-ray crystallography. Structural refinement revealed the expected Lindqvist motif, where a single vanadyl moiety was replaced by a "GaCl" cation (Figure 3, Table 2). The asymmetric unit contains one-half of the cluster, with the Lindqvist core disordered over an inversion center, coincident with the central oxygen atom (O_c). As a result of this center of inversion, the Ga-Cl moiety was modeled as disordered with one V=O moiety, in a 1:1 ratio. As expected, the newly incorporated gallium center has a pseudo-octahedral geometry. Unlike previously reported structurally characterized MPOV-alkoxide clusters, the Ga^{III}

ion sits uniformly within the vanadyl cavity. Indeed, all Ga-O bond distances in the structure of **2-V_5GaCl** resemble those of other V-O_b and V-O_c distances within this cluster, and other POV-alkoxides reported in the literature.

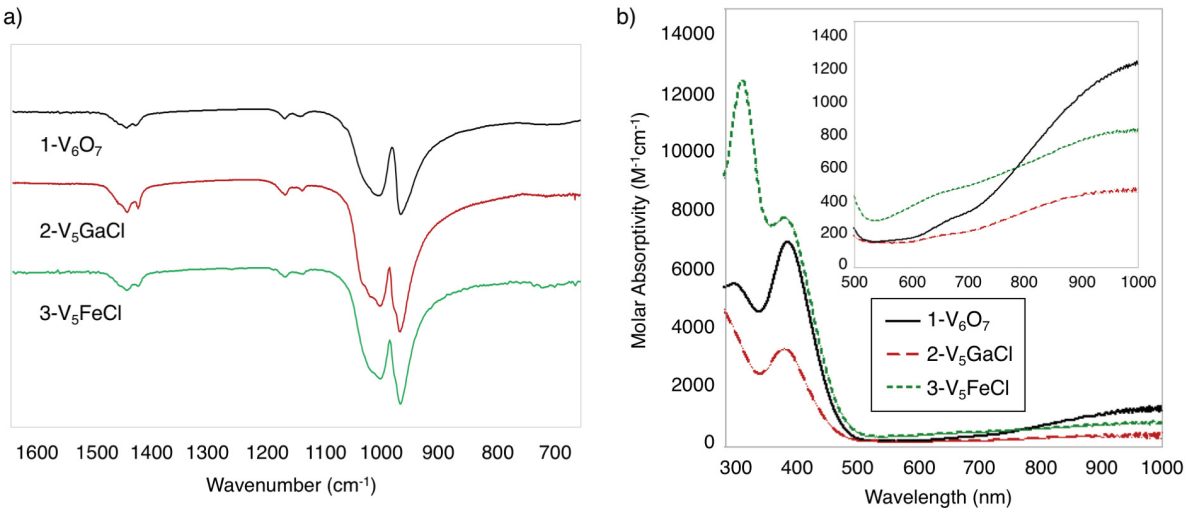

Figure 2. Spectroscopic characterization of MPOV-alkoxide clusters: (a) Infrared spectrum of **1-V_6O_7**, **2-V_5GaCl**, and **3-V_5FeCl**; (b) electronic absorption spectrum of complexes **1-V_6O_7**, **2-V_5GaCl**, and **3-V_5FeCl** collected in acetonitrile at 21 °C. The inset shows the low-energy region of the spectrum to more clearly illustrate intervalence charge transfer bands.

Table 4. IR data for complexes **2-V_5GaCl**, **3-V_5FeCl**, and **4-V_6O_6Cl** as compare to iron- and titanium-functionalized POV-alkoxide clusters previously reported by our laboratory

Compound	**$\nu(O_b\text{-}CH_3)$ (cm^{-1})**	**$\nu(V{=}O_t)$ (cm^{-1})**	**Ref**
2-V_5GaCl	1003	969	*this work*
3-V_5FeCl	1003	969	*this work*
4-V_6O_6Cl	1042	986	*this work*
$[V_5O_6(OCH_3)_{12}Fe]X$			
X = $OClO_3^-$	1007	979	45
$OSO_2CF_3^-$	1012	974	33
OCN^-	1016	976	45
$[V_5O_6Ti(OCH_3)_{13}]^-$	1040	958	34

O_b = oxygen atom of the bridging methoxide ligands; O_t = terminal oxygen atom of the vanadyl moieties.

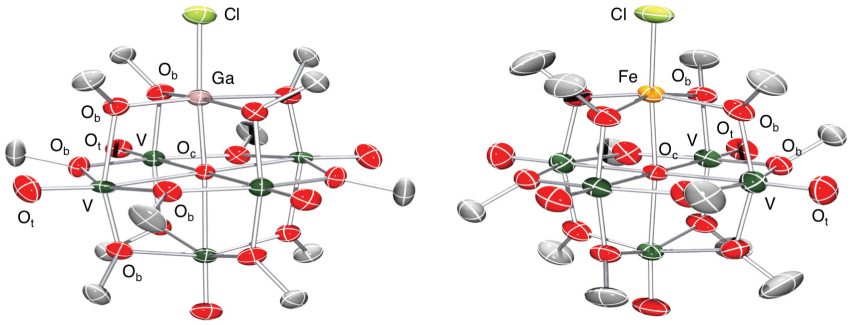

Figure 3. Molecular structure of **2-V_5GaCl** and **3-V_5FeCl** shown with 30% probability ellipsoids. Hydrogen atoms have been removed for clarity.

Table 2. Structural parameters of **1-V_6O_7**,[34] **2-V_5GaCl,** and **3-V_5FeCl**.

Bond	$[V_6O_7(OCH_3)_{12}]$ **1-V_6O_7** (Å)	$[V_5O_6(OCH_3)_{12}GaCl]$ **2-V_5GaCl** (Å) M = Ga	$[V_5O_6(OCH_3)_{12}FeCl]$ **3-V_5FeCl** (Å) M = Fe
M-Cl	--	2.162(12)	2.242(8)
M-O_b (avg)	--	1.977	1.987
M-O_c	--	2.225(11)	2.215(8)
V=O_t (avg)	1.588	1.627	1.587
V-O_b (avg)	1.962	1.966	1.963
V-O_c (avg)	2.2807	2.2801	2.3015

O_b = oxygen atom of the bridging methoxide ligands; O_c = central μ^6-oxygen atom; O_t = terminal oxygen atom of the vanadyl moieties.

Complex **2-V_5GaCl** is the *first* example of a gallium-functionalized POV cluster. Furthermore, there are only a few examples in the literature of tungstate,[44-47] molybdate,[48] and niobate[49] clusters with gallium incorporated into the structure. The majority of these heterometallic assemblies display a canonical Keggin-type morphology, $[GaM_{12}O_{40}]^{n-}$ (M=Mo, W), with the Ga^{III} ion embedded in the center of the cluster. These gallium-functionalized Keggin motifs have been demonstrated to support the formation of stable Lacunary structures that can subsequently bind other transition metal centers.[44-45, 47] Other structural configurations have also been obtained

through incorporation of Ga^{III} into Lacunary structures of well-studied Keggin- and Dawson-type polyoxotungstates.[46] While these gallium-functionalized clusters display promising structural diversity, systematic study of the electronic and physical properties of these clusters remains underdeveloped.

In order to evaluate the consequences of gallium-functionalization on the redox properties of the POV-alkoxide cluster, the cyclic voltammogram (CV) of **2-V_5GaCl** was collected in acetonitrile with $[Bu_4N][PF_6]$ as the supporting electrolyte (Figure 4, Table 3). The CV of **2-V_5GaCl** contains four quasi-reversible redox events ($E_{1/2}$ = -0.57, -0.11, 0.43, and 0.97 V vs. Ag/Ag^+), with peak-to-peak separation ($\Delta E_{1/2}$ ~0.60 V) consistent with vanadium-based, redox chemistry.[30-34, 42] Measurement of the open circuit potential (OCP) of complex **2-V_5GaCl** indicates that zero current occurs at +0.12 V, placing the neutral charge state of the cluster, with an electronic distribution of $[V^{IV}_3V^{V}_2Ga^{III}]$, between the second and third redox couples. Therefore, the four events can be assigned to successive single-electron processes localized to the POV-alkoxide scaffold, spanning clusters with oxidation state distributions ranging from $[V^{IV}_5Ga^{III}]$ to $[V^{IV}V^{V}_4Ga^{III}]$ (Table 3).

Our previous work with MPOV-alkoxide clusters has demonstrated the utility of heterometal installation for tuning the redox potentials of the cluster core.[31, 42] We have attributed the observed difference in $E_{1/2}$ values of MPOV-alkoxide clusters to variations in electron occupancy of the heterometal *d*-orbitals, demonstrating that electron population of valence orbitals effectively modulates the electrochemical profile of the cluster in its entirety. In the case of titanium-functionalization, incorporation of the electron-deficient Ti^{IV} cation results in an anodic shift of vanadium-based redox events of the heterometallic POV-alkoxide by approximately +0.5 V. This change in redox potentials was attributed to the ability of the electron deficient, $3d^0$ Ti^{IV}

center to pull electron density away from the POV-alkoxide scaffold, thus supporting vanadium reduction at less-reducing potentials. In contrast, substitution of a vanadyl moiety for a five-coordinate ferric cation results in a cathodic shift of redox events by approximately -0.2 V (in comparison to **1-V_6O_7**), thus the electron-rich, $3d^5$ iron center affords a more-reducing POV-alkoxide cluster.

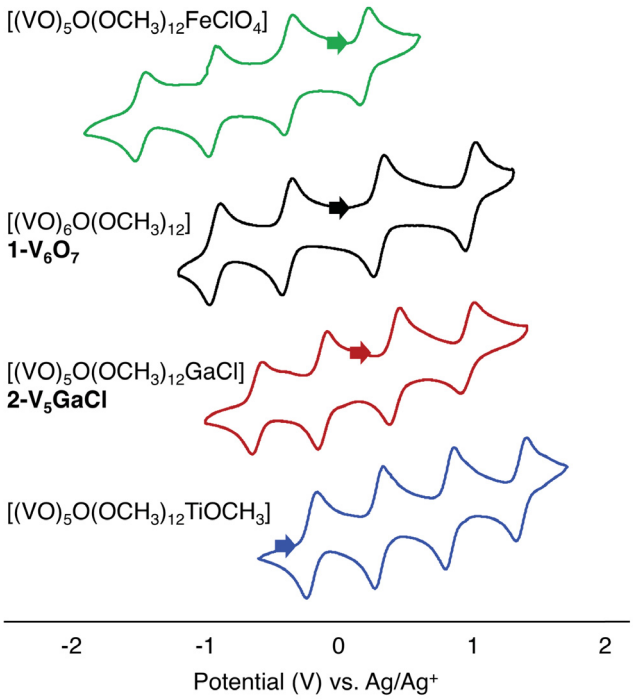

Figure 4. Cyclic voltammogram of complexes **1-V_6O_7** (black), **2-V_5GaCl** (red), $[V_5O_6(OCH_3)_{12}Fe]^+$ (green) and $[V_5O_6Ti(OCH_3)_{13}]^-$ (blue), collected in acetonitrile with 0.1 M $[Bu_4N][PF_6]$ as the supporting electrolyte (ν = 200 mV s^{-1}).

Table 3. Redox potentials obtained from the Cyclic Voltammogram of **2-V_5GaCl**.

Redox Process (Electron Distribution of Metal Ions)	$E_{1/2}$ **vs** $Ag^{0/+}$ **in** CH_3CN
$[V^{IV}V^{V}_4Ga^{III}]^{2+} + e^- \rightleftharpoons [V^{IV}_2V^{V}_3Ga^{III}]^{1+}$	+0.97 V
$[V^{IV}_2V^{V}_3Ga^{III}]^{1+} + e^- \rightleftharpoons [V^{IV}_3V^{V}_2Ga^{III}]$	+0.43 V
$[V^{IV}_3V^{V}_2Ga^{III}] + e^- \rightleftharpoons [V^{IV}_4V^{V}Ga^{III}]^{1-}$	-0.11 V
$[V^{IV}_4V^{V}Ga^{III}]^{1-} + e^- \rightleftharpoons [V^{IV}_5Ga^{III}]^{2-}$	-0.57 V

Although the $3d^{10}$ Ga^{III} cation can be considered an electron-rich heteroatom, gallium-functionalization imparts an anodic shift on the redox events of the POV-alkoxide cluster, similar to electron-deficient transition metal ions (Figure 4). Therefore, alternative electronic effects must be invoked to justify the observed shifts in the electrochemical profile of the heterometal-functionalized POV-alkoxide assemblies. Looking to other bimetallic[50-53] and multimetallic[54-60] systems, containing closed-shell, redox-inactive metal cations [e.g. group 1, group 2, group 13, and lanthanide metals], heterometal substitution uniformly results in shifts in the redox events toward more-oxidizing potentials. A notable exception is the series of lanthanide-substituted manganese-cubane clusters, $[LLn^{III}Mn^{IV}_3O_4(OAc)_3(DMF)_n]OTf$; n = 2 when Ln = Ce, Nd, Eu, Gd, Tb, Dy, Yb, Lu; n = 3 for Ln = La; L = 1,3,5-tris(2-di(2'-pyridyl)hydroxymethylphenyl)benzene], reported by Agapie and coworkers.[57] Compared to the analogous homometallic tetramanganese cubane cluster, which displays a $Mn^{III}Mn^{IV}_3/Mn^{III}_2Mn^{IV}_2$ redox event at ~0.3 V (vs Fc/Fc^+ in N,N-dimethylacetamide),[58-59] the lanthanide-functionalized clusters afford significant cathodic instead of anodic shifts in the $E_{1/2}$ value of the Mn^{IV}/Mn^{III} couple ($\Delta E_{1/2}$ = -0.35 to -0.49 V). The authors justify the shifts in $E_{1/2}$ by correlating the observed values to the Lewis acidity of the installed redox-innocent ions. Using pKa values of the aqueous lanthanide ions as a benchmark for their Lewis acidity,[61] Agapie and coworkers demonstrated that as the pKa of the heteroion increased, a corresponding cathodic shift of the Mn^{III}/Mn^{IV} redox couples was observed. Thus, the replacement of the Mn^{III} center of the all-manganese cubane with the more Lewis basic lanthanide ions results in a shift in the redox profile towards more reducing potentials.

With the aim to evaluate whether the Lewis acidic properties of the heterometal cations correlate to the redox profile of our POV-alkoxide systems in a similar manner, we compared the aqueous pKa values of V^{IV}, Fe^{III}, Ti^{IV}, and Ga^{III} to the redox properties of their respective POV-

alkoxide clusters. For the hexavanadate cluster, we treated a V^{IV} vanadyl unit as the heterometal for two reasons: 1) the aqueous pKa value of the V^{IV} vanadyl ion is well established and 2) the charge distribution of the remaining five vanadium centers compares favorably to the other heterometallic clusters. The $E_{1/2}$ values for the $[V^{IV}{}_5M]/[V^{IV}{}_4V^{V}M]$ (M = V^{IV}, Ti^{IV}, Zr^{IV}, Hf^{IV}, Ga^{III}, and Fe^{III}) redox couple of each cluster were plotted against the aqueous pKa values of the respective heterometal ion reported in the literature (Figure 5, Table S1).[61] A similar pKa analysis was performed for the other redox events, and is summarized in the supporting information (Figure S8, Table S1). As observed in the case of the manganese-oxide cubane clusters, a negative linear relationship between the pKa and the potential of the $E_{1/2}$ values holds for all redox events of the hexavanadate, group 4-functionalized, and gallium-functionalized clusters. Curiously, the iron-functionalized cluster is an exception to this trend. Though the pKa values of Ga^{III} and Fe^{III} are quite similar (2.7 and 3.0, respectively), the Ga^{III} ion induces the expected oxidative shift in the redox potential compared to the more Lewis basic vanadyl ion, while the open-shell, Fe^{III} ion shifts the redox peak cathodically. This suggests that incorporation of Fe^{III} affords a more reducing POV-alkoxide assembly, which is supported by the fact that upon reduction to the dianionic charge state, this cluster has been shown to access a V^{III} ion within the POV framework.[42] As such, in contrast to its closed-shell congeners, the presence of the five-coordinate ferric ion appears to stabilize lower oxidation states of vanadium ions within the cluster in a manner not explicitly predicted by the Lewis acidity of the heteroion.

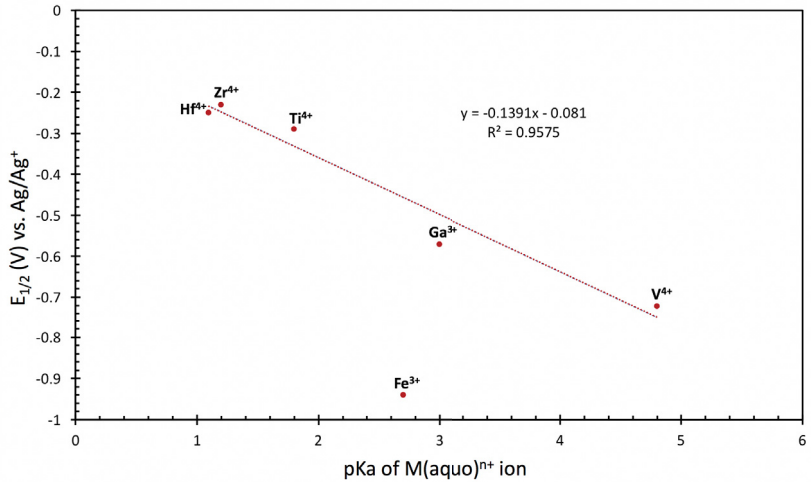

Figure 5. Plot of the redox potentials of the $V^{IV}_5M/V^{IV}_4V^{V}M$ redox couple (M=V^{IV}, Ti^{IV}, Zr^{IV}, Hf^{IV}, Ga^{III}, and Fe^{III}) of the POV-alkoxide clusters (acetonitrile, 0.1 M $[Bu_4N][PF_6]$ as the supporting electrolyte, referenced to Ag/Ag^+) versus the pKa of the corresponding aqueous heteroions as a measure of Lewis acidity. The data point for iron-functionalized cluster (Fe^{3+}) was excluded from the linear fitting analysis as the $E_{1/2}$ value is anomalously low.

Synthesis of an Iron-functionalized POV-alkoxide cluster.

With the GaPOV-alkoxide cluster in hand, attempts to access the iron-functionalized derivative, $[V_5O_6(OCH_3)_{12}FeCl]$ (**3-V_5FeCl**), under identical reaction conditions were pursued. Interest in this cluster stemmed from the hypothesis that metal ions with similar ionic radii and charge (e.g. Ga^{III} and Fe^{III}) could potentially be incorporated using similar methodologies, despite differences in the valence electron configurations of these metal ions (Ga^{III} = $3d^{10}$ while Fe^{III} = $3d^5$). Following the prescriptive synthesis for the formation of **2-V_5GaCl** (*vide supra)*, two equivalents of $FeCl_3$ were added to a 5:1 mixture of $VO(OCH_3)_3$ and $NaBH_4$ in THF. After 20 hours at 65 °C, ^{1}H NMR of the crude reaction showed complete consumption of the mononuclear, vanadium starting material, and formation of a three-peak pattern, similar to that observed for **2-V_5GaCl** (Figure S9). However, ESI-MS of this mixture (Figure S9) revealed formation of $[V_4O_5(OCH_3)_{12}(FeCl)_2]$ (*m/z* = 838 amu) and $[V_5O_7(OCH_3)_{11}FeCl]$ (*m/z* = 799 amu), with only a small amount of the desired **3-V_5FeCl** cluster (*m/z* = 814 amu).

In our previous work, observation of the di-iron functionalized POV-alkoxide cluster at early time points and low temperatures ultimately gives way to the formation of the mono-iron species with prolonged heating. In accordance with these results, the reaction mixture was left to heat for 92 hr, affording an increase in the ratio of **3-V_5FeCl** to the di-iron-functionalized species (Figure S10). To completely eliminate formation of di-iron POV-alkoxide, and maximize the yield of **3-V_5FeCl**, elevating the reaction temperature was explored. As predicted, raising the temperature to 85 °C over the course of two days allowed for successful isolation of the iron-functionalized analog, **3-V_5FeCl** (Scheme 1; Figures S11-S12)**.** This result is noteworthy, as the generation of an iron-functionalized POV-alkoxide cluster has previously only been achieved using ferrous precursors.[30, 42]

The ^{1}H NMR spectrum of **3-V_5FeCl** contains two paramagnetically shifted resonances (13.32 and 23.23 ppm), consistent with the those of the previously reported FePOV-alkoxide clusters $[V^{IV}_3V^{V}_2O_6(OCH_3)_{12}Fe^{III}]X$ (X = $OClO_3^-$, $OSO_2CF_3^-$, and OCN^-) (Figure S11). Furthermore, the IR spectrum of **3-V_5FeCl** (Figure 2a) contains the characteristic ν(O-CH_3) and ν(V=O) bands with values of 1003 and 968 cm^{-1}, respectively, resembling values reported for $[V^{IV}_3V^{V}_2O_6(OCH_3)_{12}Fe]ClO_4$ (1007, 979 cm^{-1}) and $[V^{IV}_3V^{V}_2O_6(OCH_3)_{12}Fe]OTf$ (1012, 974 cm^{-1}). Notably, these features in the IR spectrum of **3-V_5FeCl** are nearly identical to the values of ν(O-CH_3) and ν(V=O) observed for **2-V_5GaCl** (1003, 969 cm^{-1}), suggesting that these heterometallic POV-alkoxide clusters share similar structural and electronic properties. Indeed, crystallographic analysis on single, dark green crystals of complex **3-V_5FeCl**, grown from concentrated methanol solution at -30 °C (Figure 3, Table 2), confirmed that the structure of **3-V_5FeCl** is isotypic to that of **2-V_5GaCl**.

The electronic structure of **3-V_5FeCl** was further interrogated *via* electronic absorption spectroscopy. The spectrum of the FePOV-alkoxide cluster contains three features, located at 308 (1.1 x 10^4 $M^{-1}cm^{-1}$), 382 (8.2 x 10^3 $M^{-1}cm^{-1}$), and 990 nm (9.5 x 10^2 $M^{-1}cm^{-1}$) (Figure 2b). Absorptions located at 382 and 990 nm are attributed to the $d_{xy}(V^{IV}) \rightarrow d_{x^2-y^2}(V^V)$ and $d_{xy}(V^{IV}) \rightarrow d_{xy}(V^V)$ electronic transitions, consistent with analogous IVCT bands observed in the spectrum of **2-V_5GaCl**. The presence of this pair of electronic transitions confirms a mixed-valent oxidation state distribution of vanadyl ions (V^{IV}/V^V) across the Lindqvist core. In the spectrum of **3-V_5FeCl**, an additional absorption is observed at 308 nm. Similar features have been reported in "M-Cl" substituted POV-alkoxide clusters, including $[V_5O_6(OCH_3)_{12}FeCl]^+$ (302 nm, 2.29 x 10^4 $M^{-1}cm^{-1}$) and $[V_5O_6(OCH_3)_{12}TiCl]^-$ (383, 2.5 x 10^3 $M^{-1}cm^{-1}$), and can be assigned to a $Cl: \rightarrow M$ ligand-to-metal charge transfer event.[42, 62] Although complex **2-V_5GaCl** also has a terminal chloride ligand bound to the heterometal ion, LMCT is not observed in the spectrum of **3-V_5FeCl**. This major difference in the absorption profiles of these two otherwise isotypic complexes is due to the full *d*-shell of the Ga^{III} ion ($3d^{10}$ electronic configuration), which prevents charge transfer from the chloride ligand to the metal center.

To more rigorously assign the oxidation state of the iron center in complex **3-V_5FeCl**, ^{57}Fe Mössbauer spectroscopy was performed. The Mössbauer spectrum collected at 80 K (Figure 6, Table 4) was fit to a single iron species, with parameters of δ = 0.48 mm/s and ΔE_q = 0.97 mm/s. These values are consistent with previously reported 6-coordinate, high-spin ferric centers within a POV-alkoxide scaffold (Table 4). Taken together, these results confirm a charge distribution of $[V^{IV}_3V^V_2Fe^{III}]$ for the neutral **3-V_5FeCl** cluster.

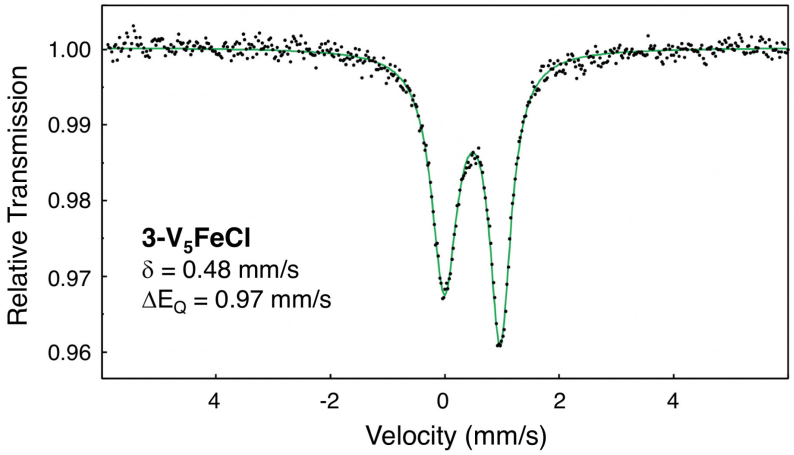

Figure 6. ^{57}Fe Mössbauer spectrum of **3-V_5FeCl** collected at 80 K (solid sample). The data (dots) and the fit (solid line) are displayed, and the Mössbauer fit parameters are given in Table 4.

Table 4. ^{57}Fe Mössbauer spectroscopic parameters of **3-V_5FeCl** compared to other iron-functionalized POV-alkoxide clusters

Compound	CN[a]	δ (mm s^{-1})	ΔE_Q (mm s^{-1})	Reference
3-V_5FeCl	6	0.48[b]	0.97[b]	*This work*
$[V_5O_6(OCH_3)_{12}FeOClO_3]$	6	0.54[c]	0.80[c]	45
	5	0.52[c]	1.32[c]	45
$[V_5O_6(OCH_3)_{12}FeOCN]$	6	0.49[c]	0.79[c]	45
$[V_5O_6(OCH_3)_{12}FeCl][SO_3CF_3]$	6	0.50[c]	1.01[c]	45

[a]Coordination number around the iron center; [b]Mössbauer spectrum measured of solid sample of **3-V_5FeCl** at 80K; [c]Mössbauer spectrum measured of solid sample of FePOV-alkoxide cluster at 5K.

*Attempts to extend synthesis of **2-V_5GaCl** to other group 13 metalloids*

Following the successful isolation of both gallium- and iron-functionalized POV-alkoxide clusters, we sought to test the generality of these reaction conditions by attempting to extend this chemistry to the installation other group 13 metalloid ions. In previous work from our laboratory, successful installation of larger group 4 metal ions was achieved through the substitution of Zr^{4+} and Hf^{4+} molecular precursors [$M(O^tBu)_4$; M = Zr, Hf] under identical reaction conditions established for the formation of a TiPOV-alkoxide cluster.[31] As such, we pursued the synthesis of

an indium-functionalized POV-alkoxide cluster, based on the hypothesis that the group 13 metalloid ions would behave in a similar fashion to their group 4 congeners.

Modeling the successful reaction conditions for formation of **2-V_5GaCl**, $InCl_3$ was used in place of $GaCl_3$. Unfortunately, the ESI-MS of the crude reaction mixture did not contain any signals corresponding to indium-installed POV cluster or the hexavanadate congeners. The ^{1}H NMR of this mixture also showed only very weak, paramagnetically broadened signals (Figure S13). Reducing the amount of $InCl_3$ to a single equivalent did produce some indium-functionalized cluster ([$V_5O_7(OCH_3)_{11}InCl$], *m/z* = 858 amu), as observed by ESI-MS (Figure S14). However, the major product detected in the ESI-MS of the crude reaction mixture was a cluster with a mass (*m/z*) of 809 amu, with an isotopic distribution consistent with the formula "[$V_6O_6(OCH_3)_{12}Cl$]" (Figure S15).

The "[$V_6O_6(OCH_3)_{12}Cl$]" cluster crashes out of the tetrahydrofuran reaction mixture as a bright blue solid, and thus can be isolated by collecting the solid *via* filtration in moderate yield (32%, based on V). Analysis of the product by ^{1}H NMR spectroscopy (Figure S16) revealed four sharp peaks in the diamagnetic region (0.96, 1.34, 1.58, and 3.07 ppm), suggesting the presence of a tetrabutylammonium cation as a counterion for the cluster. Indeed, elemental analysis of a sample recrystallized from methanol confirmed the empirical formula of the cluster to be [Bu_4N][$V_6O_6(OCH_3)_{12}Cl$] (**4-V_6O_6Cl**). One paramagnetically broadened resonance was also observed in the ^{1}H NMR spectrum of **4-V_6O_6Cl** (7.99 ppm), and was assigned to the bridging methoxide ligands of the POV-alkoxide cluster. The presence of a single resonance suggests formation of a highly symmetric molecular assembly, precluding formation of a Lindqvist structure with a single terminal vanadyl moiety replaced by a "V-Cl" cation.

In considering potential structures for complex **4-V_6O_6Cl**, we proposed formation of a Lindqvist-type hexavanadate cluster, with the central μ^6-oxo ligand replaced by a chloride ion. Central chloride ions have reported previously for POV clusters, principally by Streb and coworkers in their $[Bu_4N]_3[(C_2H_8N)_2V_{12}O_{32}Cl]$, $\{V_{12}\}$, assemblies.[18] Our structural hypothesis was deemed plausible through characterization of **4-V_6O_6Cl** by FT-IR and electronic absorption spectroscopy (Figure 7). Charge-balancing of the molecular assembly suggests complex **4-V_6O_6Cl** possesses an isovalent V^{IV} charge distribution. Accordingly, two intense IR bands were observed, with energies corresponding to the anticipated $\nu(O_b\text{-}CH_3)$ (1042 cm^{-1}) and $\nu(V{=}O)$ (986 cm^{-1}) stretching frequencies of the hexavanadate core (Figure 7a, Table 1). These values resemble those reported for isovalent V^{IV} POV-alkoxide assemblies, namely $[V^{IV}_6O_7(OCH_3)_{12}]^{2-}$ (1083, 946 cm^{-1}, respectively) and $[V^{IV}_5TiO_6(OCH_3)_{13}]^-$ (1040, 958 cm^{-1}, respectively). The higher energy of the $\nu(V{=}O_t)$ band was attributed to the presence of a central μ^6-chloride ion. The monoanionic charge of this central atom would result in weaker interactions with the six vanadyl ions, shortening the $V{=}O_t$ bonds of the cluster. Further support for the isovalent Lindqvist assembly was noted in the absorption spectrum of **4-V_6O_6Cl**, which contains a low intensity band at 578 nm (ε= 56 $M^{-1}cm^{-1}$), consistent with a forbidden $d_{xy}(V^{IV}) \rightarrow d_{x^2-y^2}(V^{IV})$ excitation (Figure 7b).

However, discrepancies in spectroscopic data collected for complex **4-V_6O_6Cl** pointed toward the possibility of an alternative structure of the POV-alkoxide assembly. Additional electronic transitions were observed in the electronic absorption spectrum of **4-V_6O_6Cl** at 390 nm (ε = 107 $M^{-1}cm^{-1}$) and 788 nm (ε= 94 $M^{-1}cm^{-1}$), values that have not been noted previously in Lindqvist POV-alkoxide assemblies. While this spectroscopic difference could possibly be attributed to electronic disturbances of the cluster core as a result of substitution of a chloride ion for the central oxygen atom, it suggested that a distinct molecular arrangement may be responsible

for this observation. Electrochemical analysis of complex **4-V_6O_6Cl** *via* cyclic voltammetry further highlighted differences in electronic structure (Figure S17). In the case of traditional Lindqvist POV-alkoxide clusters, four, evenly-spaced reversible redox events are typically observed, as noted in Figure 4. However, when the electrochemical profile of complex **4-V_6O_6Cl** was interrogated by CV, no reversible redox processes were detected.

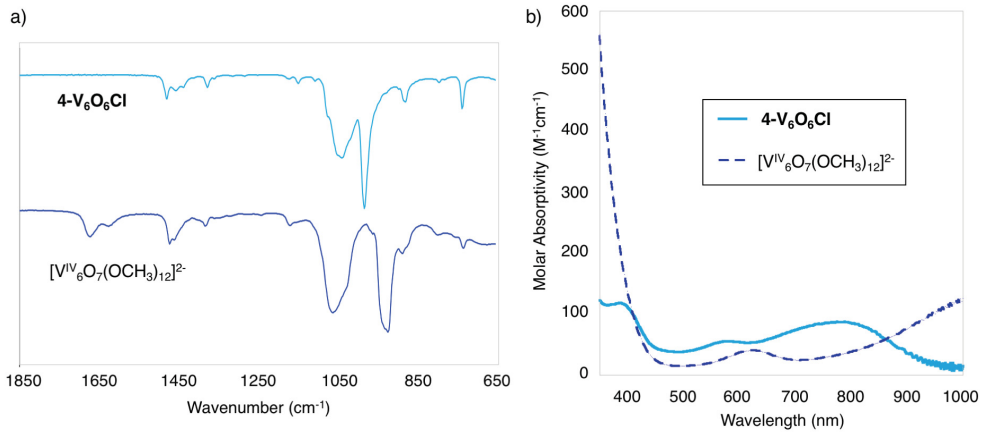

Figure 7. Spectroscopic characterization of **4-V_6O_6Cl**: (a) Infrared spectrum, plotted against the fully reduced hexavanadate cluster, $[V^{IV}{}_6O_7(OCH_3)_{12}]^{2-}$; (b) electronic absorption spectrum plotted against the spectrum of $[V^{IV}{}_6O_7(OCH_3)_{12}]^{2-}$, collected in acetonitrile at 21 °C.

To determine the molecular structure of **4-V_6O_6Cl**, crystals suitable for X-ray analysis were grown from a concentrated acetonitrile solution. Instead of the anticipated Lindqvist structure, six $[(V^{IV}O)(OCH_3)_2]$ subunits form a cyclic, metallocrown-like assembly, surrounding an encapsulated chloride anion (Figure 8, Table 5). The asymmetric unit contains a chloride ion located on an inversion center, resulting in only one-half of the vanadium cluster (3 "$VO(OCH_3)_2$" subunits) occupying crystallographically distinct positions. The bridging methoxides are oriented inward in an alternating fashion, so that three of the methoxides on each face form close contacts with the central chloride atom (~3.107 Å $Cl\cdots O_{methoxide}$, ~3.043 Å $Cl\cdots H\text{-}C_{methoxide}$). A similar ring-like POV cluster, $[Bu_4N]_2[V_8O_8(OCH_3)_{16}(C_2O_4)]$, has been shown to form during the reaction of

rhodizonic acid with $[Bu_4N]_3[H_3V_{10}O_{28}]$ in methanol (Table 5).[63] The structural parameters of the six-member and the eight-member POV rings are almost identical. However, the way in which the vanadyl rings interact with their central anions are notably different. In the case of the oxalate cluster, $[Bu_4N]_2[V_8O_8(OCH_3)_{16}(C_2O_4)]$, each oxygen atom of the encapsulated anion coordinates directly to two vanadium ions, with an average V-O bond distance of 2.394 Å. The presence of these V-O bonds between the POV-alkoxide cluster and the central oxalate anion result in a 6-coordinate geometry for all vanadium centers within the assembly. In contrast, the vanadyl ions of **4-V_6O_6Cl** do not display any direct bonding interactions with the central chloride (V···Cl = 3.0407(4) – 3.0762(4) Å, typical V-Cl distances range from 2.282 – 2.391 Å[62, 64-67]), resulting in pseudo-square pyramidal geometries for each vanadium center.

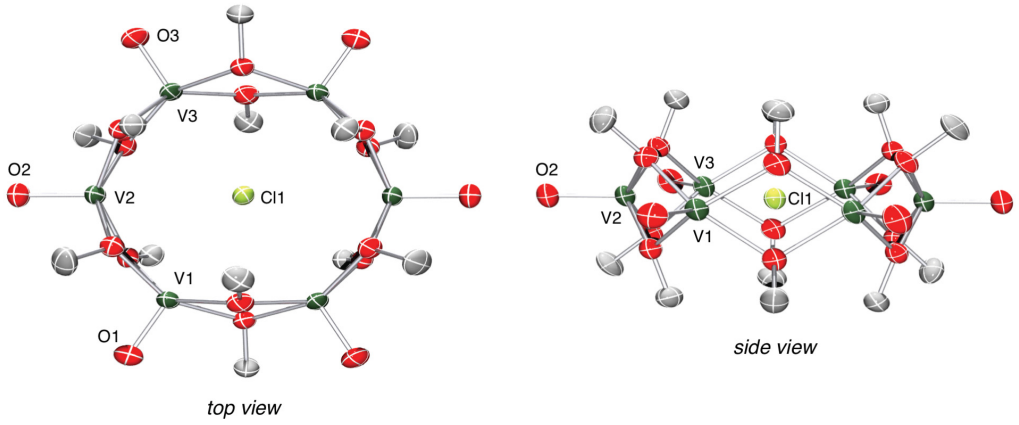

Figure 8. Molecular structure of **4-V_6O_6Cl** shown with 30% probability ellipsoids. The tetrabutylammonium counter ion, hydrogen atoms and residual solvent molecules have been removed for clarity.

Though **4-V_6O_6Cl** is structurally similar to $[Bu_4N]_2[V_8O_8(OCH_3)_{16}(C_2O_4)]$, the chloride-containing cluster appears to form *via* a mechanism more similar to the pseudo-Lacunary, "barrel-shaped" $\{V_{12}\}$ cluster,[19] reported by Streb and co-workers.[18] This dodecavanadate cluster was theorized to assemble *via* templating two six-member POV rings around a central chloride anion.

Interestingly, generation of the $\{V_{12}\}$ cluster was only observed in the presence of the group 13 ions, suggesting that these metalloids play an important role during cluster assembly.

Table 5. Structural parameters of **4-V_6O_6Cl** and $[Bu_4N]_2[V_8O_8(OCH_3)_{16}(C_2O_4)]$[63]

Bonds or Angles	$[Bu_4N][V_6O_6(OCH_3)_{12}Cl]$ **4-V_6O_6Cl**	$[Bu_4N]_2[V_8O_8(OCH_3)_{16}(C_2O_4)]$
V=O_t (avg)	1.594 Å	1.596(8) Å
V-O_b (avg)	1.986 Å	2.011 Å
V-$O_{oxalate}$ (avg)	--	2.394(8) Å
V…Cl (avg)	3.059 Å	--
V-O_b-V (avg)	100.8°	92.3(3)° and 99.6(3)°

O_b = oxygen atom of the bridging methoxide ligands; O_t = terminal oxygen atom of the vanadyl moieties; $O_{oxalate}$ = oxygen atoms of oxalate anion.

To complete the series of group 13 elements explored in this work, attempts at incorporating an Al^{III} ion into the POV-alkoxide cluster was pursued. This served the additional purpose of assessing whether the size of In^{III} (0.800 Å) may preclude facile installation of this heterometal within the Lindqvist structure.[41] No cluster formation was observed when two equivalents of $AlCl_3$ was reacted with a 5:1 mixture of $VO(OCH_3)_3$ and $[Bu_4N][BH_4]$ in THF at 65 °C. Full consumption of the $VO(OCH_3)_3$ precursor was noted by ^1H NMR spectroscopy. However, a lack of signals in both the paramagnetic region of the ^1H NMR spectrum and absence of features in the ESI-MS suggested no cluster formation occurs under these reaction conditions.

CONCLUSION.

In this report, we present the synthesis and characterization of gallium- and iron-functionalized POV-alkoxide clusters. Notably, we were able to access both heterometal-functionalized POV-alkoxide clusters through similar chemical reactions. This result is exciting,

given that the electronically distinct Ga^{III} and Fe^{III} ions, which are similar in size and charge, can incorporated into the POV assembly in spite of differences in their electronic structures and accessible redox states. However, the installation of other group 13 metal centers, such as indium, could not be realized using these parameters. Future studies will focus on accessing a diverse range of heterometallic POV-alkoxide clusters with the goal of gaining a better understanding on how the properties of the installed heterometal affect the electronic, structural, and reactivity profiles of the clusters.

EXPERIMENTAL SECTION.

General Considerations. All manipulations were carried out in the absence of water and oxygen in a UniLab MBraun inert atmosphere glovebox under an atmosphere of dinitrogen. Glassware was oven dried for a minimum of 4 hours and cooled in an evacuated antechamber prior to use in the drybox. Celite 545 (J. T. Baker) was dried in a Schlenk flask for at least 14 hours at 150 °C under vacuum prior to use. 3 Å molecular sieves (Fisher Scientific) were activated using the same drying method. Anhydrous methanol was purchased from Sigma-Aldrich and stored over activated 3 Å molecular sieves. Anhydrous dibutyl ether was purchased from Sigma-Aldrich and used as received. All other solvents were dried and deoxygenated on a Glass Contour System (Pure Process Technology, LLC) and stored over activated 3 Å molecular sieves. $GaCl_3$, $FeCl_3$, and $InCl_3$ were purchased from Strem Chemicals, Inc., and used as received. $NaBH_4$ and $[Bu_4N][BH_4]$ were purchased from Sigma-Aldrich and used as received. $[Bu_4N][PF_6]$ was also purchased from Sigma-Aldrich and recrystallized three times from hot methanol, and stored under dynamic vacuum in the glovebox prior to use. $VO(OCH_3)_3$ was prepared according to literature precedent.[33]

^1H NMR spectra were recorded on a Bruker DPX-500 MHz spectrometer locked on the signal of deuterated solvents. All chemical shifts were reported relative to the peak of residual ^1H

signal in the deuterated solvents. $CDCl_3$ and CD_3CN were purchased from Cambridge Isotope Laboratories, degassed by three freeze-pump-thaw cycles, and stored over activated 3 Å molecular sieves. Infrared (FT-IR, ATR) spectra of complexes were recorded on a Shimadzu IRAffinity-1 Fourier Transform Infrared spectrophotometer and were reported in wavenumbers (cm^{-1}). Electronic absorption measurements were recorded at room temperature in anhydrous acetonitrile in a sealed 1 cm quartz cuvette with an Agilent Cary 60 UV-Vis spectrophotometer. Mass spectrometry analyses were performed on an Advion expression^L Compact Mass Spectrometer equipped with an electrospray probe and an ion-trap mass analyzer. Direct injection analysis was employed in all cases with a sample solution in acetonitrile. Single crystals were mounted on the tip of a thin glass optical fiber (goniometer head) and mounted on a XtaLab Synergy-S Dualflex diffractometer equipped with a HyPix-6000He HPC area detector for data collection at 243.00(10) K (**2-V_5GaCl** and **3-V_5FeCl**) and 100.1(1) K (**4-V_6O_6Cl**). The structures were solved using ShelXT[2] and refined using ShelXL.[3] Elemental analyses were performed on a PerkinElmer 2400 Series II Analyzer, at the CENTC Elemental Analysis Facility, University of Rochester.

Cyclic Voltammetry measurements were carried out at room temperature in a nitrogen filled glove box, using a Bio-Logic SP 150 potentiostat/galvanostat and the EC-lab software suite. Cyclic voltammograms were recorded using a glassy carbon working electrode (ø = 3.0 mm) and a Pt wire auxiliary electrode, both purchased from CH Instruments, USA. An Ag/Ag^+ non-aqueous reference electrode with 0.01 M $AgNO_3$ in 0.05 M $[Bu_4N][PF_6]$ in CH_3CN was purchased from Bio-Logic and used as the reference electrode for all cyclic voltammetry measurements. The cyclic voltammograms of complexes **2-V_5GaCl**, **3-V_5FeCl,** and **4-V_6O_6Cl** were collected in 0.1 M $[Bu_4N][PF_6]$ solutions in dry acetonitrile. All redox events were referenced against $Ag^{+/0}$ redox couple.

^{57}Fe Mössbauer spectroscopy was run on an isolated solid sample of **3-V_5FeCl,** made from natural abundance iron. Samples were prepared in an inert-atmosphere glovebox. After loading the solid sample into a Delrin Mössbauer cup, the sample was frozen using liquid nitrogen. ^{57}Fe Mössbauer measurements were performed using a SEE Co. MS4 Mössbauer spectrometer integrated with a Janis SVT-400T He/N_2 cryostat for measurements at 80 K. Isomer shifts were determined relative to α-iron at 298 K. All Mössbauer spectra were fit using the program *WMoss* (SEE Co.)

*Synthesis of [$V_5O_6(OCH_3)_{12}GaCl$] (**2-V_5GaCl**)*. In a glovebox, a 150 mL pressure vessel was charged with $VO(OCH_3)_3$ (1.217 g, 7.60 mmol, 5.0 equiv.) and 60 mL tetrahydrofuran. Solid $NaBH_4$ (0.058 g, 1.54 mmol, 1.0 equiv.) was then added in small portions. Once a dark green solution formed, 0.537 g $GaCl_3$ (3.05 mmol, 2.0 equiv.) was added. The vessel was sealed, removed from the glovebox, and heated at 65 °C in an oil bath for 20 hours, affording a green solution and pale precipitate. The vessel was returned to the glovebox, and the reaction mixture was filtered over a bed of Celite (1.0 cm) on a medium-porosity frit. Volatiles were removed under reduced pressure, and the resulting dark green solid was triturated with diethyl ether. The solid was extracted with dichloromethane and filtered over a bed of Celite (1.0 cm) on a medium-porosity frit. After the dichloromethane was removed under reduced pressure, complex **2-V_5GaCl** was isolated as a dark green solid (0.480 g, 0.58 mmol, 38% yield based on V). More product could be crystallized from the diethyl ether trituration by concentrating the solution to half the original volume, and placing the solution in a -30 °C freezer overnight (0.162 g, 0.19 mmol, 13% yield based on V). Total yield: 0.641 g (0.77 mmol, 51% yield based on V) was isolated. Crystals suitable for X-ray analysis were grown from a concentrated *n*-butyl ether solution at -30 °C. ^{1}H NMR (500 MHz, CD_3CN): δ = 10.20 (fwhh = 247 Hz), 17.40 (fwhh = 413 Hz), 24.03 (fwhh = 822

Hz). FT-IR (ATR, cm^{-1}): 1003 (O_b—CH_3), 969 (V=O_t). UV-Vis [CH_3CN; λ, nm (ε, $1x10^3$ M^{-1} cm^{-1})]: 378 (3.36), 990 (0.35). Elemental analysis calculated for $C_{12}H_{36}O_{18}V_5GaCl$ (%) (MW = 828.29 g mol^{-1}): C, 17.40; H, 4.38; Found (%): C, 17.669; H, 4.105.

*Synthesis of $[V_5O_6(OCH_3)_{12}FeCl]$ (**3-V_5FeCl**).* In a glovebox, a 150 mL pressure vessel was charged with $VO(OCH_3)_3$ (1.2018 g, 7.51 mmol, 5.0 equiv.) and 60 mL tetrahydrofuran. Solid $NaBH_4$ (0.057 g, 1.50 mmol, 1.0 equiv.) was then added in small portions. Once gas evolution ceased and a dark green solution formed, $FeCl_3$ (0.487 g, 3.00 mmol, 2.0 equiv.) was added. The vessel was sealed and heated in an 85 °C oil bath for 48 hours, affording a green solution and pale precipitate. The vessel was returned to the glovebox, and the reaction mixture was filtered over a bed of Celite (1.0 cm) on a medium-porosity frit. Volatiles were removed under reduced pressure, and the resulting dark green solid was extracted with dichloromethane (2 mL x 3). The dichloromethane solution was filtered over a bed of Celite (1.0 cm) on a medium-porosity frit, and the solvent was removed. The resulting solid was extracted with diethyl ether (10 mL x 3), and the diethyl ether solution was filtered over a bed of Celite (1.0 cm) on a medium-porosity frit. The solvent was removed, and the resulting solid was triturated with methanol (4 mL x 3), affording **3-V_5FeCl** as a dark green solid [0.3131g, 0.38 mmol, 26% yield based on $VO(OCH_3)_3$]. Crystals suitable for x-ray analysis were grown from a concentrated methanol solution at -30 °C. ^{1}H NMR (500 MHz, CD_3CN): δ = 13.27 (fwhh = 506 Hz), 23.26 (fwhh = 301 Hz). FT-IR (ATR, cm^{-1}): 1003 (O_b—CH_3), 968 (V=O_t). UV-Vis [CH_3CN; λ, nm (ε, 1 x 10^2 M^{-1} cm^{-1})]: 308 (111), 382 (81.6), 990 (9.50). Elemental analysis calculated for $C_{12}H_{36}O_{18}V_5FeCl$ (%) (MW = 814.41 g mol^{-1}): C, 17.70; H, 4.46. Found: C, 17.855; H, 4.315%.

*Synthesis of $[(VO)_6(OCH_3)_{12}]$•$[^nBu_4N]Cl$ (**4-V_6O_6Cl**).* In a glovebox, a 48 mL pressure vessel was charged with $VO(OCH_3)_3$ (0.361 g, 2.25 mmol, 5.0 equiv.) and 18 mL tetrahydrofuran. Solid

$[Bu_4N][BH_4]$ (0.116 g, 0.45 mmol, 1.0 equiv.) was then added in small portions. Once gas evolution ceased and a dark green solution formed, 0.100 g $InCl_3$ (0.45 mmol, 1.0 equiv.) was added. The vessel was sealed, removed from the glovebox, and heated at 65 °C in an oil bath for 20 hours, affording a green solution and pale precipitate. The vessel was returned to the glovebox, and the precipitate was collected as a bright blue solid by filtration over a bed of Celite (1.0 cm) on a medium-porosity glass frit. The solid was triturated with fresh tetrahydrofuran and extracted with acetonitrile. Volatiles were removed under vacuum, and the product, **4-V_6O_6Cl**, was recrystallized from methanol at -30 °C (0.124 g, 32% based on V). Crystals of complex **4-V_6O_6Cl**, suitable for X-ray analysis, were grown from a concentrated acetonitrile solution at -30 °C. ^{1}H NMR (500 MHz, CD_3CN): δ = 0.96 (fwhh = 31 Hz), 1.34 (fwhh = 39 Hz), 1.58 (fwhh = 39 Hz), 3.07 (fwhh = 39 Hz), 7.99 (fwhh = 722 Hz) ppm. FT-IR (ATR, cm^{-1}): 1042 (O_b—CH_3), 986 (V=O_t). UV-Vis [CH_3CN; λ, nm (ε, M^{-1} cm^{-1})]: 390 (1.19 x 10^2), 578 (0.56 x 10^2), 788 (0.88 x 10^2). Elemental analysis calculated for $C_{28}H_{72}NO_{18}V_6Cl$ (%) (MW = 1051.97 g mol^{-1}): C, 31.97; H, 6.90; N, 1.33. Found (%): C, 31.990; H, 6.867; N, 1.182.

APPENDIX A. Supplementary data

The supporting information file contains spectral data (^{1}H NMR, ESI-MS) for complexes **2-V_5GaCl**, **3-V_5FeCl**, and **4-V_6O_6Cl**. Additionally, tabulated crystallographic parameters of compelxes **2-V_5GaCl**, **3-V_5FeCl**, and **4-V_6O_6Cl** can be found in the supporting information file. The entries CCDC 1856903 (**2-V_5GaCl**), CCDC 1856904 (**3-V_5FeCl**), and CCDC 1856905 (**4-V_6O_6Cl**) contain the supplementary crystallographic data for the compounds listed in parentheses. These data can be obtained, free of charge online, or from the Cambridge Crystallographic Data

Centre, 12 Union Road, Cambridge CB2 1EZ, UK; fax (+44) 1223-336-033; or e-mail: deposit@ccdc.cam.ac.uk.

ACKNOWLEDGMENT

The authors would like to acknowledge Robert Love Jr. for support in the synthesis of starting materials and the Neidig Laboratory for access to their Mössbauer spectrometer. This research was funded by the National Science Foundation through grants CHE-1653195 and CHE-1725028 (MRI). The authors also acknowledge generous financial support from the University of Rochester for this work.

REFERENCES

1. D. E. Katsoulis, Chem. Rev. 98 (1998) 359.
2. L. De-Liang, T. Ryo, L. Cronin, Angew. Chem. Int. Ed. 49 (2010) 1736.
3. D.-L. Long, E. Burkholder, L. Cronin, Chem. Soc. Rev. 36 (2007) 105.
4. S.-S. Wang, G.-Y. Yang, Chem. Rev. 115 (2015) 4893.
5. C. L. Hill, J. Mol. Catal. A: Chemical 262 (2007) 2.
6. I. A. Weinstock, R. E. Schreiber, R. Neumann, Chem. Rev. 118 (2018) 2680.
7. X. Zhao, S. Zhang, J. Yan, L. Li, G. Wu, W. Shi, G. Yang, N. Guan, P. Cheng, Inorg. Chem. 57 (2018) 5030.
8. J. J. Walsh, A. M. Bond, R. J. Forster, T. E. Keyes, Coord. Chem. Rev. 306 (2016) 217.
9. M. Genovese, K. Lian, Current Opinion in Solid State and Materials Science 19 (2015) 126.
10. A. Sakamoto, K. Unoura, H. Nabika, J. Phys. Chem. C 122 (2018) 1404.
11. A. Boulmier, X. Feng, O. Oms, P. Mialane, E. Rivière, C. J. Shin, J. Yao, T. Kubo, T. Furuta, E. Oldfield, A. Dolbecq, Inorg. Chem. 56 (2017) 7558.
12. A. Müller, F. Peters, M. T. Pope, D. Gatteschi, Chem. Rev. 98 (1998) 239.
13. J. M. Clemente-Juan, E. Coronado, A. Gaita-Ariño, Chem. Soc. Rev. 41 (2012) 7464.
14. L. E. VanGelder, A. M. Kosswattaarachchi, P. L. Forrestel, T. R. Cook, E. M. Matson, Chem. Sci. 9 (2018) 1692.
15. L. E. VanGelder, E. M. Matson, J. Mat. Chem. A 6 (2018) 13874.
16. Q. Li, L. Zhang, J. Dai, H. Tang, Q. Li, H. Xue, H. Pang, Chem. Eng. J. 351 (2018) 441.
17. Y. Hayashi, Coord. Chem. Rev. 255 (2011) 2270.
18. K. Kastner, J. T. Margraf, T. Clark, C. Streb, Chem. Eur. J. 20 (2014) 12269.
19. M. H. Anjass, K. Kastner, F. Nägele, M. Ringenberg, J. F. Boas, J. Zhang, A. M. Bond, T. Jacob, C. Streb, Angew. Chem. Int. Ed. 56 (2017) 14749.

20. J. M. Cameron, G. N. Newton, C. Busche, D.-L. Long, H. Oshio, L. Cronin, Chem. Commun. 49 (2013) 3395.
21. V. Day, W. Klemperer, O. Yaghi, J. Am. Chem. Soc. 111 (1989) 5959.
22. J. Forster, B. Rösner, R. H. Fink, L. C. Nye, I. Ivanovic-Burmazovic, K. Kastner, J. Tucher, C. Streb. Chem. Sci. 4 (2013) 418.
23. K. Kastner, B. Puscher, C. Streb, Chem. Commun. 49 (2013) 140.
24. M. Nishio, S. Inami, M. Katayama, K. Ozutsumi, Y. Hayashi, Inorg. Chem. 51 (2012) 784.
25. I Shinnosuke, N. Masaki, H. Yoshihito, I. Kiyoshi, K. Hiroyuki, S. Tatsuya, Eur. J. Inorg. Chem. 34 (2009) 5253.
26. T. Kurata, A. Uehara, Y. Hayashi, K. Isobe, Inorg. Chem. 44 (2005) 2524.
27. C. M. Flynn Jr., M. T. Pope, Inorg. Chem. 9 (1970) 2009.
28. C. M. Flynn Jr., M. T. Pope, J. Am. Chem. Soc. 92 (1970) 85.
29. F. Li, R. L. Meyer, S. H. Carpenter, L. E. VanGelder, A. W. Nichols, C. W. Machan, M. L. Neidig, E. M. Matson, Chem. Sci. 9 (2018) 6379.
30. F. Li, L. E. VanGelder, W. W. Brennessel, E. M. Matson, Inorg. Chem. 55 (2016) 7332.
31. L. E. VanGelder, W. W. Brennessel, E. M. Matson, Dalton Trans. 47 (2018) 3698.
32. C. Daniel, H. Hartl, J. Am. Chem. Soc. 127 (2005) 13978.
33. C. Daniel, H. Hartl, J. Am. Chem. Soc. 131 (2009) 5101.
34. J. Spandl, C. Daniel, I. Brudgam, H. Hartl, Angew. Chem. Int. Ed. 42 (2003) 1163.
35. O. Nachtigall, J. Spandl, Chem. Eur. J. 24 (2018) 2785.
36. J. Zhang, Y. Huang, G. Li, Y. Wei, Coord. Chem. Rev. (2017).
37. Y. Kaneko, M. Thoendel, O. Olakanmi, B. E. Britigan, P. K. Singh, J. Clinical Invest. 117 (2007) 877.
38. C. R. Chitambar, M. M. Al-Gizawiy, H. S. Alhajala, K. R. Pechman, J. P. Wereley, R. Wujek, P. A. Clark, J. S. Kuo, W. E. Antholine, K. M. Schmainda, Mol. Cancer Ther. (2018).
39. C. R. Chitambar, Pharma. Res. 115 (2017) 56.
40. C. R. Chitambar, Mol. Cell Res. 1863 (2016) 2044.
41. R. D. Shannon, Acta. Cryst. A 32 (1976) 751.
42. F. Li, S H. Carpenter, R. F. Higgins, M. G. Hitt, W. W. Brennessel, M. G. Ferrier, S. K. Cary, J. S. Lezama-Pacheco, J. T. Wright, B. W. Stein, M. P. Shores, M. L. Neidig, S. A. Kozimor, E. M. Matson, Inorg. Chem. 56 (2017) 7065.
43. M. B. Robin, P. Day, Adv. Inorg. Chem. Radiochem. 10 (1968) 247.
44. D. Daniel, L. E. Melanie, K. Bernt, Eur. J. Inorg. Chem. (2005) 1542.
45. B. Lihua, P. Jun, C. Yaguang, L. Jingfu, Q. Lunyu, Polyhedron 13 (1994) 2421.
46. F. Zonnevijlle, C. M. Tourne, G. F. Tourne, Inorg. Chem. 21 (1982) 2742.
47. G. F. Tourné, C. M. Tourné, A. Schouten, Acta Cryst. B 38 (1982) 1414.
48. S.. Himeno, S. Murata, K. Eda, Dalton Trans. (2009) 6114.
49. Y. Hou, T. M. Alam, M. A. Rodriguez, M. Nyman, Chem. Commun. 48 (2012) 6004.
50. A. Kumar, D. Lionetti, V. W. Day, J. D. Blakemore, Chem. Eur. J. 24 (2018) 141.
51. R. C. Cammarota, C. C. Lu, J. Am. Chem. Soc. 137 (2015) 12486.
52. T. Chantarojsiri, J. W. Ziller, J. Y. Yang, Chem. Sci. 9 (2018) 2567.
53. A. H. Reath, J. W. Ziller, C. Tsay, A. J. Ryan, J. Y. Yang, Inorg. Chem. 56 (2017) 3713.
54. D. E. Herbert, D. Lionetti, J. Rittle, T. Agapie, J. Am. Chem. Soc. 135 (2013) 19075.
55. S. Hong, Y.-M. Lee, M. Sankaralingam, A. K. Vardhaman, Y. J. Park, K.-B. Cho, T. Ogura, R. Sarani, S. Fukuzumi, W. Nam, J. Am. Chem. Soc. 138 (2016) 8523.
56. V. Krewald, F. Nesse, D. A. Pantazis, Phys. Chem. Chem. Phys 18 (2016) 10739.

57. P.-H. Lin, M. K. Takase, T. Agapie, Inorg. Chem. 54 (2015) 59.
58. E. Y. Tsui, T. Agapie, Proc. Natl. Acad. Sci. 110 (2013) 10084.
59. E. Y. Tsui, R. Tran, J. Yano, T. Agapie, Nat. Chem. 5 (2013) 293.
60. J. S. Kanady, J. L. Mendoza-Cortes, E. Y. Tsui, R. J. Nielsen, W. A. Goddard, T. Agapie, J. Am. Chem. Soc. 135 (2013) 1073.
61. D. D. Perrin, *Ionization Constants of Inorganic Acids and Bases in Aqueous Solution*. Pergamon: Oxford, U.K. (1982).
62. L. E. VanGelder, P. L. Forrestel, W. W. Brennessel, E. M. Matson, Chem. Commun. 54 (2018) 6839.
63. Q. Chen, S. Liu, J. Zubieta, Inorg. Chem. 28 (1989) 4433.
64. R. Ruivo, L. G. Alves, K. Kirchner, A. M. Martins, J. Mol. Struct. 1149 (2017) 229.
65. F. Wolff, C. Lorber, R. Coukroun, B. Donnadieu, Inorg. Chem. 42 (2003) 7839.
66. C. Marquardt, C. Thoms, A. Stauber, G. Balázs, M. Bodensteiner, M. Scheer, Angew. Chem. Int. Ed. 53 (2014) 3727.
67. K.-P. Lörcher, J. Strähle, I. Walker, Z. Anorg. Allge. Chem. 452 (1979) 123.